

1 **Preliminary magnetostratigraphic results from the late Miocene Maragheh Formation, NW**
2 **Iran**

3

4 Johanna Salminen¹, Mohammad Paknia², Anu Kaakinen^{2*}, Majid Mirzaie Ataabadi³, Gholamreza
5 Zare⁴, Zahra Orak⁵ and Mikael Fortelius²

6

7 ¹Department of Physics, P.O. Box 64, University of Helsinki, Finland

8 ²Department of Geosciences and Geography, P.O. Box 64, University of Helsinki, Finland

9 ³Department of Geology, University of Zanjan, Zanjan 45371/38791, Iran

10 ⁴Department of Environment, Maragheh, Iran

11 ⁵Department of Environment, National Museum of Natural History (MMTT), Tehran, Iran

12

13 *corresponding author

14 email: anu.kaakinen@helsinki.fi; tel. +358-2941 50819; FAX +358-2941 50827

15

16 **Keywords**

17 Fossil mammals, Maragheh fauna, Turolian, Paleomagnetism, Neogene, Iran, Hominoid

18

19

20 **Abstract**

21 Maragheh in northwestern of Iran is a world famous Miocene fossil-bearing area. The area has
22 yielded classical late Miocene Turolian age fauna that has been collected and studied sporadically
23 over the last 150 years. However, the precise correlation of these sediments to the Global Time
24 Scale (GTS) has remained ambiguous. To address this, 115 levels along an approximately 27-m-
25 thick interval were collected from the middle Maragheh Formation at Dareh Gorg (Gort Daresi)
26 section. Characteristic remanent magnetization directions obtained by alternating field
27 demagnetization produce a polarity pattern that is supported by thermal demagnetization on a set
28 of sister specimens. Three polarity intervals were recognized, the middle part of the section at
29 around 15–21 m showing reversed polarity, bounded by normal polarities above and below. Based
30 on the paleontological constraints and recent K-Ar age determinations from the Maragheh Fm,
31 three correlations to the geomagnetic polarity time scale appear likely. According to these
32 correlations, recently discovered hominoid locality is correlated to C3Br.1n, C4n.1n, or to C4n.2n.
33 For a unique correlation, however, additional paleomagnetic data is required from the upper and
34 lower parts of the section.

35

36 **Introduction**

37 The Late Miocene (ca. 11.6–5 million years ago) is the time of the great expansion of the so-called
38 “Pikermian” faunas in Eurasia, characterized by open-country adapted fossil mammal
39 communities (Bernor et al. 1979, Bernor 1986; Eronen et al. 2009). Such animals including three-
40 toed horses, giraffes, antelopes, rhinoceroses, elephants, big cats, hyenas, and many other smaller
41 species roamed vast areas of Eurasia, from Spain and central-eastern Europe through the Balkans
42 and Anatolia into the western and central Asia and China (Solounias et al. 1999; Agustí & Antón
43 2002). Maragheh, one of these localities, is a world famous fossil-bearing area and has been among
44 the first localities with these faunas to be known and studied, along with Pikermi and Samos in
45 Greece. The Maragheh fauna was first reported by a Russian explorer Khanikoff in 1840 (Bernor
46 1986, Bernor et al. 1996). The subsequent expeditions by different research groups extracted
47 impressive fossil mammal collections, stored in several museums around the world (Mecquenem
48 1908, 1924–1925; Bernor 1978, 1986; Watabe 1990; Watabe & Nakaya 1991; Bernor et al. 1996;
49 see Mirzaie Ataabadi et al. 2013 for details).

50

51 Correlation of the Maragheh sequence with the Global Time Scale is mainly achieved by a
52 combination of radiometric dating techniques, including K-Ar (Erdbrink et al. 1976; Bernor et al.
53 1980; Campbell et al. 1980; Sawada et al. this issue), single grain crystal ^{40}Ar - ^{39}Ar (Swisher III
54 1996) and fission track of zircons (Kamei et al. 1977; Bernor et al. 1980), and biostratigraphy. The
55 interbedded lava flows, and ash beds and the mammalian faunas, especially the evolutionary stages
56 of the *Hipparion* species, give a late Miocene age ranging from nearly 9 Ma to less than 7.6 Ma
57 for the Maragheh fauna (Bernor et al. 1996; Mirzaie Ataabadi et al. 2013). However, the precise
58 correlation of these sediments to the Global Time Scale (GTS) has remained ambiguous due to the
59 error margins and partly due to inconsistency with stratigraphic division (Sawada et al. 2016, this
60 issue).

61

62 Only preliminary paleomagnetism has previously been applied in the Maragheh area by the Dutch
63 and Japanese groups who worked in the area in the 1970s (Erdbrink et al. 1976; Kamei et al. 1976).
64 These analyses suggest that the samples in Maragheh show stable paleomagnetic results showing
65 two magnetization polarities. However, only few levels were sampled; hence, reliable
66 magnetostratigraphical correlations with the GTS based on these sparse data were not possible.

67

68 This study focuses on the late Miocene Maragheh Fm exposed in the Dareh Gorg. The
69 volcanoclastic sediments of this interval comprise the middle part of the Maragheh Formation (Fig.
70 1). We sampled a large number of horizons from a well-exposed 27-m section for paleomagnetic
71 study covering a recently discovered hominoid locality (Suwa et al. this issue). The objective of
72 this study is to test whether a coherent magnetostratigraphic time framework can be achieved for
73 the Maragheh Formation and secondly, to provide preliminary temporal framework and tie points
74 for the Maragheh faunas and stratigraphic correlations. This is the first time that high-resolution
75 magnetostratigraphy is employed to the classical Maragheh sequence.

76

77 **Geological setting and stratigraphy**

78 The Maragheh area belongs to the Hamedan-Tabriz (HTV) volcanic belt that trends in a NW-SE
79 direction to the south of the Tabriz dextral fault (Anatolian transform fault). HTV belt was active
80 in the Miocene to Quaternary and consists mainly of acidic andesite to dacite rocks (Azizi and

81 Moinevaziri 2009; Azizi et al. 2014). The late Miocene Maragheh sequence accumulated in the
82 central part of the HTV, on the southern flank of the Mt. Sahand volcanic massif that forms a large
83 calc-alkaline volcanic complex 100 km round (Bernor 1986; Azizi & Moinevaziri 2009). Kamei
84 et al. (1977) named the entire 500–600-m-thick late Miocene sequence in the Maragheh basin as
85 Maragheh Formation, whilst later work by Campbell et al. (1980) restricted the Maragheh
86 Formation to the lowermost 300 m of volcanoclastic strata and separated the basal pyroclastic units
87 as a Basal Tuff Formation, locally exceeding 80 m in thickness. The fossiliferous beds are
88 concentrated to the lower half of the 300-m-thick Maragheh Formation, and they rest on the Basal
89 Tuff Fm with a low angular unconformity. The whole sequence is capped by Pliocene-Quaternary
90 terrace sediments, informally named as the Kerajek Formation. Campbell et al. (1980) and Bernor
91 (1986) distinguished four sedimentary facies in the Maragheh Fm with poorly sorted massive
92 siltstones comprising the bulk of deposits, pebble and cobble conglomerate, grey sandstone, and
93 breccia, and air-fall tuff accounting for the less abundant facies.

94
95 Our fieldwork focused on the middle Maragheh Fm, in Dareh Gorg (Gort Daresi or “wolf valley”),
96 located near Mordagh village ca. 15 km east-southeast from Maragheh town. Kamei et al. (1977)
97 provided the first lithostratigraphical scheme for the Dareh Gorg section and described the
98 distinctive marker beds above the Basal Tuff as Mordaq Tuff, Lower Pumice, White Fine Tuff,
99 Upper Pumice, “Scoria” Bed, Pumice Falls, Sargizeh Tuff, and Korde Deh Ash Flow, that are the
100 rudiments to the lithostratigraphic framework and correlation for this part of the Maragheh
101 Formation. We follow Kamei et al. (1977) nomenclature modified by Sakai et al. (2016, figs 2 and
102 3, this issue). Sakai et al. (2016, this issue) conducted high-resolution facies analysis in Dareh
103 Gorg and recognized nine lithofacies from the section, representing fluvial channel fills and flood
104 plain facies associations. Our field investigations focused on the interval between the “hominoid
105 locality” ca. 8 m below the “Middle Pumice” (Pumice Bed 2 of Mirzaie Atabadi et al., 2013;
106 likely the Lower Pumice of Kamei et al. 1977) and the White tuff (Fig. 2). The lithology of the
107 studied interval shows a dominance of floodplain depositional environments (cf. Sakai et al. this
108 issue), characterized by massive silty sand and sandy silt beds, commonly exhibiting paleosol
109 formation and poorly sorted texture, and a few intercalated laminated silts. A notable feature is an
110 up to 5-m-thick pumice bed (“the Middle Pumice”) comprised of stratified sand and pebble beds
111 with occasional cobble-rich horizons in the lower part while the upper part mainly exhibits well-
112 sorted laminated silts and fine sand. This unit has been interpreted as representing

113 hyperconcentrated flow deposits, likely to have been accumulated from a single flow (Sakai et al.
114 this issue).

115

116 A large number of mammalian fossils have been found in the Dareh Gorg section, including the
117 first known hominoid in Iran. In addition to the hominoid specimen, the lowermost part (hominoid
118 locality or the “field museum site”) of the studied interval has yielded proboscideans,
119 rhinocerotids, bovids, equids, giraffes, hyaenids, and primates (Mirzaie Ataabadi et al. 2016, this
120 issue). A fossil mammal site DRG1, recently excavated by the INSPE team (International Sahand
121 Paleoenvironment Expedition), occurs below a coarse-grained channel fill deposit close to the
122 “White Tuff” in the topmost part of the examined section. This unit has yielded equids and bovids,
123 including three specimens of *Oioceros* sp., as well as few rhinos, carnivores, and cervids.

124

125 **Sampling and magnetic measurements**

126

127 Oriented paleomagnetic samples were collected from 115 levels along an approximately 27-m long
128 section between the hominoid locality (“field station locality”) and White tuff. A characteristic
129 pumice layer “the Middle Pumice” formed a firm tie point between three subsections (Fig.1). All
130 samples were derived from fresh surfaces exposed by digging trenches into the outcrop. Sampling
131 focused on the fine-grained facies, coarse-grained beds were generally omitted; most of the
132 samples were extracted from massive, relatively poorly sorted silt–fine sands beds, interpreted as
133 representing debris flow and flood deposits on the floodplain (cf. Sakai et al. this issue). Average
134 sampling spacing is 21 cm varying between 1 and 75 cm, excluding the two longer gaps that exist
135 between ca 10.5 and 13.6 m due to poor outcrop conditions. The samples were taken with a
136 gasoline-powered drill using water as a coolant and oriented with both magnetic and solar
137 compasses. Drill core samples were cut in the laboratory to cylindrical specimens.

138

139 Magnetic measurements were carried out at the Solid Earth Geophysics Laboratory of the
140 University of Helsinki, Finland. Stepwise alternating field (AF) demagnetizations were done using
141 a three-axis demagnetizer with a maximum field of up to 160 mT, coupled with a 2G–DC SQUID
142 magnetometer. A set of sister specimens were chosen for thermal demagnetization. These samples
143 were first coated with sodium silicate and after that with mixture of MgO-ZrO₂ powder and water
144 to prevent breaking during the heating. After the measurement of natural remanent magnetization

145 (NRM), samples were placed into liquid nitrogen in a null field to demagnetize viscous remanent
146 magnetization (Borradaile et al. 2004), which removed 0–50% of the secondary remanence (0–
147 15% of the total NRM). Thereafter, samples were thermally demagnetized to separate the
148 characteristic remanent magnetization (ChRM) component by an argon-atmosphere ASC
149 Scientific TD48-SC furnace. Magnetization after each step was measured using 2G–DC SQUID
150 magnetometer. The AF method turned out to be more effective and provided more stable results
151 than the thermal method. The demagnetization results were analyzed using orthogonal plots,
152 stereographic projections, and demagnetization decay curves (Zijderveld 1967). Vector
153 components were isolated using principal component analysis (Kirschvink 1980) and analyzed
154 with Fisher (1953) statistics. Two quality filters for data were used. Data with calculated latitude
155 of virtual geomagnetic pole (VGP) less than 30° were separated, because of the possibility of
156 transitional geomagnetic field. In general, samples with maximum angular deviation (MAD) of
157 16° were rejected. If the data was not acceptable, a sister specimen from the same sample or from
158 the same sampling level was measured if available.

159
160 Mass normalised susceptibility of all the samples was measured with a ZH Instruments company
161 magnetic susceptibility meter using frequency of 1026 Hz and magnetic field of 320 A/m.
162 Magnetic minerals were studied by thermomagnetic analysis of selected powdered whole rock
163 specimens using an Agico KLY-3S-CS3 Kappabridge system. The low-temperature experiment,
164 in which samples were heated from -192°C to room temperature (RT 25°C), was carried out first.
165 Then, the same samples were heated from RT to 700°C and cooled back to RT in argon gas. Curie
166 temperatures were determined using the Cureval 8.0 program (www.agico.com).

167

168 **Results**

169 **Rock magnetic results**

170 *Susceptibility and NRM*

171 Bulk magnetic susceptibilities (MS) are characterized by uniformly low values (mean 2.6×10^{-6}
172 m^3/kg ; Fig. 2) and very little scattering, except for the peak values (max. $13.8 \times 10^{-6} \text{m}^3/\text{kg}$) at the
173 “Middle Pumice” level. The natural remanent magnetization (NRM) intensities vary between
174 1.1×10^{-2} and $3.1 \times 10^{-1} \text{mAm}^2/\text{kg}$ for the entire section (Fig. 2). The highest NRM values (3.1×10^{-1}
175 mAm^2/kg) were obtained for the floodplain deposits in the basal 5 m of the section whilst the
176 “Middle Pumice bed” yields similar values with the bulk of the deposits.

177

178 *Thermomagnetic properties*

179 Thermomagnetic properties of the nine selected samples were measured. All the studied samples
180 show irreversible heating and cooling curves (Fig 3). The majority of the samples show two
181 ferromagnetic phases during the heating, first one with Curie temperatures between 550 and 580°C
182 indicating magnetite and a second one with Curie temperatures between 650 and 680°C indicating
183 hematite (Dunlop & Özdemir 1997). The sample 39A shows additional ferromagnetic phase at
184 380–400°C that indicates titanomagnetite. Lower susceptibility of cooling curves shows that in
185 spite of the argon atmosphere, some of the magnetite oxidised to hematite during heating. Low-
186 temperature measurements show Verwey transition (Verwey 1939) between –157°C and –175°C
187 for samples 90A, 19A, and 64A indicating the presence of stoichiometric magnetite.

188

189

190 **Paleomagnetic results**

191 The natural remanent magnetization (NRM) intensity decay curves after alternating field (AF)
192 demagnetization show that the initial intensity decays rapidly to half of its original intensity with
193 median destructive fields (MDF) less than 25 mT, so that for the 40% of the samples, MDF is less
194 than 7.5 mT, pointing to magnetite as the dominant carrier of remanent magnetization. Progressive
195 AF demagnetization reveals two components: an initial low coercivity component was obtained
196 between 0 and 15 mT peak fields. A high coercivity characteristic remanent magnetization
197 (ChRM) component was isolated between 15 and 120/160 mT with vector diagrams decaying to
198 origin (Fig. 4) further supporting magnetite as the carrier of ChRM. However, since
199 thermomagnetic analysis of samples show the presence of both magnetite and hematite, eleven
200 samples were selected for thermal demagnetization in order to verify the carrier of ChRM.
201 Intensity decay curves of thermal demagnetization show unblocking temperatures close to 580°C,
202 supporting that magnetite carries the ChRM. Thermal demagnetization data also reveal two
203 components. The low-temperature component is removed in temperatures less than 300°C and the
204 high-temperature component is separated between 300°C and 580°C/640°C (Fig. 5). The
205 maximum angular deviation (MAD) values for thermally demagnetized samples were less than
206 16° only for two samples.

207

208 Analyzed declination and inclination results are plotted in stratigraphic order in Fig. 2. In total,
209 143 specimens from 131 separate drill core samples were analysed. One hundred of these show
210 well-defined ChRM directions with MAD less than 16° and are indicated with solid circles. Results
211 from twenty-three specimens show VGP latitude less than 30° , which could indicate transitional
212 geomagnetic field and are indicated with a white triangle. In addition, twenty specimens show
213 MAD values higher than 16° and are plotted with a grey square, but seventeen of these show
214 otherwise clear polarities (Fig. 2).

215
216 All the ChRM directions obtained are shown in the Fig. 6. Paleomagnetic reversal test was used
217 to determine whether the average normal and reversed NRM directions are statistically antipodal
218 within a given confidence limit (McFadden & McElhinny 1990). The mean direction for seventy-
219 eight normal samples is $D= 356.5^\circ$, $I= 45.4^\circ$ with $\alpha_{95}= 5.9^\circ$, $K= 8.3$, and $R= 68.7$, and the mean
220 direction for twenty-two reversed samples is $D= 171.7^\circ$, $I= -47.7^\circ$ with $\alpha_{95}=17.5^\circ$, $K= 4.3$, and
221 $R= 16.3$ (Fig. 6). The test shows that the antipode of the mean of the reversed polarity sites and the
222 mean of the normal polarity sites pass the test with classification Rc (observed angle is 4.0° and
223 critical angle in 14.8°). Passage of the reversal test indicates that ChRM directions do not have
224 contamination due to secondary magnetization.

225
226 **Discussion and conclusions**

227 *Previous paleomagnetic studies*

228 Two previous paleomagnetic studies have been carried out for the Maragheh Formation in 1970s
229 by Erdbrink et al. (1976) and Kamei et al. (1977). Erdbrink et al. (1976) sampled different
230 tuffaceous and other volcanic layers at ten levels along a 79.5-m composite section in Maragheh.
231 The samples were subjected to alternating field demagnetization with maximum fields of 300 mT
232 for test samples and 150 mT for rest of the samples. Seven horizons provided reliable results
233 showing normal polarities for the lowermost samples and reversed polarities for the overlying
234 levels. Kamei et al. (1977) further continued paleomagnetic studies by sampling nine levels at
235 Dareh Gorg section from coarse biotite tuff below the Ignimbritic tuff (Mordaq) and spanning up
236 to Korde deh ash flow far above the Upper pumice. According to Kamei et al. (1977), reasonable
237 results were obtained from four sites: a reversed polarity from the coarse Biotite tuff below the
238 Ignimbritic tuff and normal polarities for the Ignimbritic tuff, White fine tuff, and for Korde deh
239 ash flow. However, our results show that the 8 mT alternating field demagnetization used by

240 Kamei et al. (1977) does not adequately separate ChRM magnetization component, since some of
241 the samples required fields up to 15 mT to clean the viscous component. Therefore, the obtained
242 normal polarities in Kamei et al. (1977) may represent the direction of the present Earth's magnetic
243 field at the sampling site ($D: 50.5^\circ$, $I: 56.9^\circ$). Based on these sparse paleomagnetic data, it was not
244 possible to draw any conclusions about the age of the section, but they nevertheless demonstrate
245 that the material is suitable for paleomagnetic study.

246

247 *Paleomagnetism and magnetozones*

248 Two magnetization components were obtained during the paleomagnetic analyses. First one is a
249 low coercivity and a low-temperature viscous component and the second one is a higher coercivity
250 and a high-temperature characteristic remanent magnetization component (ChRM) carried by
251 nearly stoichiometric magnetite in majority of the studied samples. This is evidenced by median
252 destructive fields less than 20 mT for majority of the samples, unblocking temperatures of 580°C,
253 Curie temperatures between 550°C and 580°C, and obtained Verwey transitions. Based on the
254 obtained polarities, three magnetozones can be defined (Fig. 2). The base of the section (0–13.6
255 m), including the Middle Pumice, shows a normal polarity while the magnetization of overlying
256 samples at 13.60 to 14.30 m show unstable and at 14.30 to 15.15 m transitional field from normal
257 to reversed polarity. A reversed polarity occurs at the 15.55–20.65-m level and the uppermost
258 interval up to the White tuff comprises of normal polarity.

259

260 *Earlier geochronology and correlation of magnetozones to the ATNTS*

261 Different Pumice beds of Maragheh Formation have been dated by fission track of zircons (Kamei
262 et al. 1977; Bernor et al. 1980) by K-Ar using plagioclase and hornblende (Erdbrink et al. 1976;
263 Bernor et al. 1980; Campbell et al. 1980; Sawada et al. 2016, this issue) and by ^{40}Ar - ^{39}Ar using
264 plagioclase (Swisher III 1996). These individual radiometric age determinations with their error
265 limits are shown in Figure 7 and Table 1 and discussed briefly here for correlating the obtained
266 magnetozones, but more extensively by Sawada et al. (2016, this issue). Erdbrink et al. (1976)
267 provided K-Ar age of 12.9 ± 0.7 Ma for the Ignimbritic tuff and age of 2.5 ± 0.5 Ma for the
268 uppermost part of the Maragheh Formation. Later, this range of 10 Myr in ages for the Maragheh
269 formation has been narrowed down to ca. 2 Myr using K-Ar (Bernor et al. 1980; Campbell et al.
270 1980; Sawada et al. this issue), fission track (Kamei et al. 1977; Bernor et al. 1980), and ^{40}Ar - ^{39}Ar
271 ages (Swisher III 1996).

272

273 The recently obtained mean value of hornblende and plagioclase ages of Sawada et al. (2016, this
274 issue) bracket the Mordaq tuff to 8.41–7.87 Ma. The mean values of mineral ages of the Lower
275 Pumice Beds are 7.54 ± 0.22 Ma (A) and 6.95 ± 0.28 Ma (B), and of the Upper Pumice $6.96 \pm$
276 0.31 Ma. The mean hornblende and plagioclase K-Ar age of the Middle Pumice (7.87 ± 0.29 Ma)
277 is older than those for the Lower Pumice and therefore not consistent with the stratigraphy. Based
278 on similar geochemical major and trace element composition in the two marker beds, Sawada et
279 al. (2016, this issue) suggest that pumices of the Middle Pumice bed are reworked from the
280 underlying Lower Pumice unit and the ages do not represent the accumulation age of the Middle
281 Pumice. Previous fission track (FT) zircon ages of Kamei et al. (1977) for Dareh Gorg section
282 range slightly younger ages for the marker beds but with larger error limits suggesting 8.4–5.6 Ma
283 for the Ignimbritic tuff (Mordaq tuff), 7.8–5.2 Ma for the Lower Pumice (possibly corresponds to
284 the Middle Pumice in our study; Mirzaie Ataabadi et al. 2016, this issue), and 7.9–5.3 Ma for the
285 Upper Pumice. In addition to large errors, these earlier fission track ages are subject to larger
286 uncertainties by default since the FT method has developed substantially since 1990, yet still facing
287 the problem of absolute age calibration (e.g. Turner et al. 1980; Gallagher et al. 1998; Danhara
288 and Iwano 2013). Since the radiometric age of Sawada et al. (2016, this issue) is acquired using
289 recent K-Ar technology on two different minerals and with lower error limits than in previous
290 studies, we base our correlation on these recent ages.

291

292 Using the maximum (minimum) mean mineral K-Ar age for the Lower Pumice (Upper Pumice)
293 (Fig. 7) and the biostratigraphical evidence (Bernor et al. 1996; Mirzaie Ataabadi et al. 2013), we
294 consider a correlation of our magnetostratigraphic column to the Astronomically Tuned Neogene
295 Time Scale (ATNTS) of Gradstein et al. 2012 (Fig. 2). K-Ar results (Sawada et al. 2016, this issue)
296 provide an approximate maximum age of 7.76 Ma for the Lower Pumice and a minimum age of
297 6.65 Ma for the Upper Pumice. These age constraints and the pattern of magnetozones allow
298 several possible correlations for the polarity sequence. According to these options, the polarity
299 sequence correlates between the (upper part of) chron C4n.2n and (lower part of) chron C3An.2n.
300 Consequently, the reversal could be connected to C4n.1r, C3Br.3r, C3Br.2r, C3Br.1r, or C3Ar.
301 While all correlations appear possible, we prefer placing the reversed polarity zone to C4n.1r
302 (option 1), C3Br.3r (option 2), or C3Br.1r (option 3). The resultant sedimentation accumulation
303 rates for the reversed chrons are approximately 11–15 cm/ka, agreeing well with the estimated

304 sedimentation rate of 12.5cm/ka by Mirzaie Ataabadi et al. (2013). These correlations imply that
305 the hominoid locality would fall in the upper part of normal chron 4n.2n (option 1), 4n.1n (option
306 2), or in 3Br.1n (option 3). Placing the reversed polarity zone to 3Br.2r or 3Ar would result in
307 much lower sedimentation rates (approximately 3.5 and 1.5 cm/ka, respectively) and are
308 considered less likely. Nevertheless, the accumulation rate in Maragheh is based on one
309 magnetochron only, and large variation in rates through the sequence is expected. We also
310 acknowledge that additional paleomagnetic data from the lower and upper part of the section is still
311 required to extend the section for a firmer correlation.

312

313 **Conclusions**

314 First high-resolution paleomagnetic results from the classical Maragheh sequence in NW Iran
315 provide a preliminary magnetostratigraphy for the middle Maragheh Formation in Dareh Gorg
316 section. The quality of demagnetization results on which the magnetostratigraphic pattern is
317 based is of high quality for both normal and reversed samples, and three polarity intervals are
318 recognized. Our magnetostratigraphic correlation suggests placing the recently discovered
319 hominoid locality to the upper part of the normal polarity chron C4n.2 (7.695–8.108 Ma), chron
320 C4n.1n (7.528–7.642 Ma), or C3Br.1n (7.251–7.285 Ma). We acknowledge, however, that we
321 can only propose a tentative correlation with the geological time scale. For a unique correlation,
322 a distinct reversal pattern is necessary.

323

324 **Acknowledgments**

325 Department of Environment (environment protection organization), the Government of Iran
326 permitted and facilitated this study. We would like to express our gratitude to the heads of the
327 “natural environment division” of this organization as well as those of the “office of natural history
328 museum and genetic resources” and East Azarbaijan and Maragheh branches for their support. We
329 thank field assistance by Mr. Mohammad Ali, Mr. Suleiman Zadeh, and Ms. Mansoureh
330 Hasandoost and members of the INSPE (International Sahand Palaeoenvironmental Expedition)
331 team. This paper benefited significantly from constructive suggestions from Sevket Sen, Miguel
332 Garcés, Elisabet Beamud Amorós, and the Editor-in-chief Peter Königshof. Field work in

333 Maragheh was partially supported by the Academy of Finland (project no 257850 and 264935),
334 RHOI project, Sasakawa Foundation, and Nordenskiöld samfundet.

335

336 **Conflict of Interest:** The authors declare that they have no conflict of interest.

337

338 **References**

339 Agustí, J., & Antón, M. (2002). *Mammoths, sabertooths, and hominoids: 65 million years of*
340 *mammalian evolution in Europe*. New York: Columbia University Press, 313 pp.

341

342 Azizi, H., & Moinevaziri, H. (2009). Review of the tectonic setting of Cretaceous to Quaternary
343 volcanism in northwestern Iran. *Journal of Geodynamics*, 47(4), 167–179.

344

345 Azizi, H., Asahara, Y., Tsuboi, M., Takemura K., & Razyani, S. (2014). The role of heterogenetic
346 mantle in the genesis of adakites northeast of Sanandaj, northwestern Iran. *Chemie der Erde*, 74(1),
347 87–97.

348

349 Bernor, R. L. (1978). *The Mammalian systematics, biostratigraphy and biochronology of*
350 *Maragheh and its importance for understanding late Miocene Hominoid Zoogeography and*
351 *Evolution*. Los Angeles: University of California Dissertation.

352

353 Bernor, R. L. (1986). Mammalian biostratigraphy, geochronology and zoogeographic relationships
354 of the late Miocene Maragheh fauna, Iran. *Journal of Vertebrate Paleontology* 6 (1), 76–95.

355

356 Bernor, R. L., Andrews, P. A., Solounias, N., van Couvering, J. A. (1979). The evolution of
357 “Pontian” mammal faunas: some zoogeographic, palaeoecological, and chronostratigraphic
358 considerations. *The VIIth Inter Congr Medit Neogene. Annales géologiques des Pays helléniques*
359 *hors-série, I*, 81–89.

360

361 Bernor, R. L., Woodburne, M. O., & Van Couvering, J. A. (1980). A contribution to the
362 chrolonology of some old world Miocene faunas based on Hipparionine Horses. *Geobios*, 13 (5),
363 705–739.

364

365 Bernor, R. L., Solounias, N., Swisher C. C. III, & van Couvering, J. A. (1996). The correlation of
366 three classical “Pikermian” mammal faunas — Maragheh, Samos, Pikermi — with the European
367 MN Unit System. In R.L. Bernor, V. Fahlbusch & H.-W. Mittman (Eds), *The evolution of western*
368 *Eurasian Neogene mammal faunas* (pp. 137–154). New York: Columbia University Press.

369

370 Borradaile, G. J., Luca, K., & Middleton, R. S. (2004). Low-temperature demagnetization isolates
371 stable magnetic vector components in magnetite-bearing diabase. *Geophysical Journal*
372 *International* 157 (2), 526–536.

373

374 Campbell, B. G., Amini, M. H., Bernor, R. L., Dickinson, W., Drake, R., Morris, R., Van
375 Couvering, J.A., & Van Couvering, J.A.H. (1980). Maragheh: a classical late Miocene vertebrate
376 locality in northwestern Iran. *Nature*, 287 (5785), 837–841.

377

378 Danhara, T., & Iwano, H. (2013). A review of the present state of the absolute calibration for
379 zircon fission track geochronometry using the external detector method. *Island Arc*, 22, 264–279.

380

381 de Mecquenem, R. (1908). Contribution à l’étude du gisement des vertébrés de Maragha et ses
382 environs. In J. Morgan de (Ed.), *Délégation scientifique en Perse. Annales d’Histoire Naturelle, I,*
383 *Paléontologie*, 27–79.

384

385 de Mecquenem, R. (1924). Contribution à l’étude des fossiles de Maragha. *Annales de*
386 *Paléontologie*, 13/14, 133–160.

387

388 Dunlop, D. J., & Özdemir, Ö. (1997). *Rock Magnetism: fundamentals and frontiers* (p. 573).
389 Cambridge: Cambridge University Press.

390

391 Erdbrink, D. P. B., Priem, H. N. A., Hebeda, E. H., Cup, C., Dankers, P., & Cloetingh, S. A. P. L.
392 (1976). The bone bearing beds near Maragheh in N.W. Iran. *Geology Series B*, 79(2), 85–113.

393

394 Eronen, J. T., Mirzaie Ataabadi, M., Micheels, A., Karme, A., Bernor, R. L., & Fortelius, M.
395 (2009). Distribution history and climatic controls of the Late Miocene Pikermian chronofauna.
396 *Proceedings of the National Academy of Sciences, USA*, 106(29), 11867–11871.

397
398 Fisher, R. (1953). Dispersion of a sphere. *Proceedings of the Royal Society of London*, 217 (1130),
399 295–305.
400
401 Gallagher, K., Brown, R., & Johnson, C. (1998). Fission track analysis and its applications to
402 geological problems. *Annual Reviews of Earth and Planetary Science*, 26, 519–572.
403
404 Gradstein, F. M., Ogg, J. G., Schmitz, M. D., & Ogg, G. M. (2012). *The geologic time scale*.
405 Amsterdam: Elsevier.
406
407 Kamei, T., Ikeda, J., Ishida, H., Ishida, S., Onishi, I., Partoazar, H., Sasajima, S., & Nishimura, S.
408 (1977). A general report of the geological and paleontological survey in Maragheh area, North-
409 West Iran. *Memoirs of the faculty of science, Kyoto University, Series of Geology and*
410 *Mineralogy*, XLIII (1/2), 131–143.
411
412 Kirschvink, J. L. (1980). The least-squares line and plane and the analysis of palaeomagnetic data.
413 *Geophysical Journal of the Royal Astronomical Society*, 62 (3), 699–718.
414
415 McFadden, P. L., & McElhinny, M. W. (1990). Classification of the reversal test in palaeo-
416 magnetism. *Geophysical Journal International*, 103(3), 725–729.
417
418 Mirzaie Ataabadi, M., Bernor, R. L., Kostopoulos, D., Wolf, D., Orak, Z., Zare, G., Nakaya, H.,
419 Watabe, M., & Fortelius, M. (2013). Recent advances on paleobiological research of the late
420 Miocene Maragheh fauna, northwest Iran. In X. Wang, M. Fortelius, & L. Flynn (Eds.), *Asian*
421 *Neogene mammal biostratigraphy and chronology* (pp.544–563). New York: Columbia University
422 Press.
423
424 Mirzaie Ataabadi, M., Kaakinen, A., Kunimatsu, Y., Nakaya, H., Orak, Z., Paknia, M., Sakai, T.,
425 Salminen, J., Sawada, Y., Sen, S., Suwa, G., Watabe, M., Zare, G., Zhang, Z., & Fortelius, M.,
426 (2016). The late Miocene hominoid-bearing site in Maragheh Formation, Northwest Iran. In M.
427 Mirzaie Ataabadi and M. Fortelius (Eds.), *The late Miocene Maragheh mammal fauna; results of*

428 recent multidisciplinary research. *Palaeobiodiversity and Palaeoenvironments*, 96(3). Doi:
429 10.1007/s12549-016-0241-4

430

431 Sakai, T., Zaree, G., Sawada, Y., Mirzai Ataabadi, M., & Fortelius, M. (2016). Depositional
432 environment reconstruction of the Maragheh Formation, East Azarbaijan, Northwestern Iran. In
433 M. Mirzaie Ataabadi and M. Fortelius (Eds.), *The late Miocene Maragheh mammal fauna; results*
434 *of recent multidisciplinary research. Palaeobiodiversity and Palaeoenvironments*, 96(3) Doi:
435 10.1007/s12549-016-0238-z

436

437 Sawada, G., Zaree, G., Sakai, T., Itaya, T., Yagi, K., Hyodo, H., Imaizumi, M., Mirzaie Ataabadi,
438 M., & Fortelius, M. (2016). K-Ar ages and petrology of the late Miocene pumices from the
439 Maragheh Formation, northwest Iran. In M. Mirzaie Ataabadi and M. Fortelius (Eds.), *The late*
440 *Miocene Maragheh mammal fauna; results of recent multidisciplinary research. Palaeobiodiversity*
441 *and Palaeoenvironments*, 96(3) DOI: 10.1007/s12549-016-0232-5

442

443 Solounias, N., Plavcan, J. M., Quade, J. & Witmer, L. (1999). The paleoecology of the Pikermian
444 Biome and the savanna myth. In J. Agustí, L. Rook, & P. Andrews (Eds.), *The evolution of*
445 *Neogene terrestrial ecosystems in Europe* (pp 436–453). Cambridge: Cambridge University Press.

446

447 Suwa, G., Kunitatsu, Y., Mirzai Ataabadi, M., Orak, Z., Sasaki, T. and Fortelius, M. (2016). The
448 first hominoid from the Maragheh Formation, Iran. In M. Mirzaie Ataabadi and M. Fortelius
449 (Eds.), *The late Miocene Maragheh mammal fauna; results of recent multidisciplinary research.*
450 *Palaeobiodiversity and Palaeoenvironments*, 96(3) Doi: 10.1007/s12549-016-0234-3

451

452 Swisher, C. C., III (1996). “New $^{40}\text{Ar}/^{39}\text{Ar}$ dates and their contribution toward a revised
453 chronology for the late Miocene of Europe and west Asia. In R. L. Bernor, V. Fahlbusch & H. W.
454 Mittmann (Eds.), *The evolution of western Eurasian Neogene mammal faunas* (pp. 64–77). New
455 York: Columbia University Press.

456

457 Turner, D. L., Triplehorn, D. M., Naesser, C. W., & Wolfe, J. A., 1980. Radiometric dating of ash
458 partings in Alaskan coal beds and upper Tertiary paleobotanical stages. *Geology*, 8, 92–96.

459

460 Verwey, E. J. W. (1939). Electronic conduction of magnetite (Fe_3O_4) and its transition point at low
461 temperatures. *Nature*, 144(3642), 327–328.

462

463 Watabe, M. (1990). Fossil bovids (Artiodactyla, Mammalia) from Maragheh (Turolian, late
464 Miocene), Northwest Iran. *Annual Report Historical Museum Hokkaido*, 18, 19–55.

465

466 Watabe, M. & Nakaya, H. (1991). Phylogenetic significance of the postcranial skeletons of the
467 hipparions from Maragheh (Late Miocene), Northwest Iran. *Memoirs of the Faculty of Science,*
468 *Kyoto University, Series of Geology & Mineralogy*, 56 (1–2), 11–53.

469

470 Zijdeveld, J. D. A. (1967). A.C. demagnetization of rocks: analysis of results. In: D. W. Collinson,
471 K. M. Creer, & Runcorn, S. K. (Eds.), *Methods in paleomagnetism* (pp. 254–286). Elsevier,
472 Amsterdam

473

474 **Figure captions**

475

476 Figure 1. a – Satellite image (Google Earth) of the study area. b – The study site at Dareh Gorg
477 and the sampled subsections a–c. The Middle Pumice and the underlying paleosol were used as
478 marker beds in lithostratigraphical correlation

479

480 Figure 2. Lithological column, natural remanent magnetization (*NRM*), magnetic susceptibility,
481 declination (*Decl*) and inclination (*Incl*) of characteristic remanent component and interpreted
482 magnetostratigraphic polarity for Maragheh. In the polarity column, *black (white)* denotes normal
483 (reversed) polarity. *Grey shaded zones* represent transitional or undefined polarity. Positions of
484 Middle Pumice (*MP*), White Tuff (*WT*), and fossil localities are indicated. Suggested correlations
485 of the magnetostratigraphy of the middle Maragheh Fm to the Astronomically Tuned Neogene
486 Time Scale (*ATNTS*) of the geological time scale 2012 (Gradstein et al. 2012) together with
487 minimum and maximum mean mineral K-Ar ages for the Upper Pumice (*UP*) and Lower Pumice
488 (*LP*) (cf. Sawada et al. 2016, this issue) are shown on the right column

489

490 Figure 3. Thermomagnetic curves (susceptibility vs. temperature) for samples from different
491 lithologies at the Maragheh. Specimens were heated from room temperature up to 700°C (*red,*
492 *solid curve*) and cooled back to room temperature (*blue, dotted curve*) in argon gas

493

494 Figure 4. Examples of demagnetization behaviour during alternating field (AF) demagnetization.
495 Shown are orthogonal (Zijderveld, 1964) demagnetization diagrams. *Solid (open) symbols* refer to
496 the projection on the horizontal (vertical) plane in geographic coordinates. Number at
497 demagnetization step denotes the AF value in mT

498

499 Figure 5. Examples of demagnetization behaviour during thermal (TH) demagnetization. Shown
500 are orthogonal (Zijderveld 1964) demagnetization diagrams (*in left side*) and intensity decay curve
501 (*in right side*). *Solid (open) symbols* refer to the projection on the horizontal (vertical) plane in
502 geographic coordinates. Number at demagnetization step denotes the TH value in °C

503

504 Figure 6. Equal area projection of characteristic remanent magnetization directions for Maragheh.
505 *Solid (open) symbols* are directions in the lower (upper) hemisphere. The means are shown with

506 *stars with circle* of 95% confidence. The antipode of the mean of the reversed polarity sites is
507 within 4° of the mean of the normal polarity site. Data pass the reversal test of paleomagnetic
508 stability (McFadden and McElhinny 1990)

509

510 Figure 7. Radiometric ages and magnetostratigraphic polarities for the Dareh Gorg section
511 obtained in the earlier studies of Kamei et al. (1977); Bernor et al. (1980); Swisher III (1996);
512 Sawada et al. (2016), this issue. Dated key beds are drawn in stratigraphical order. The 27-m long
513 section sampled in this study, and the location of field station is indicated in the column

514

515

516 **Table captions**

517

518 Table 1. Radiometric ages obtained for the Dareh Gorg section

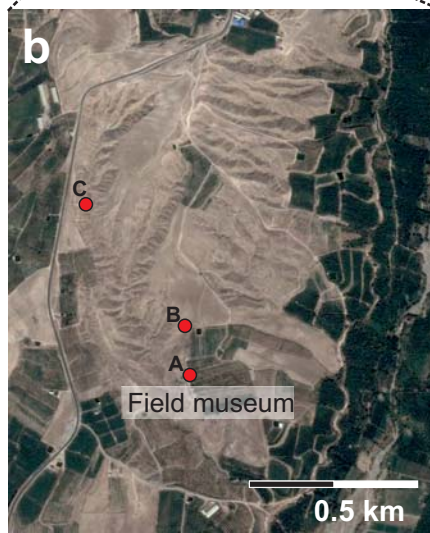
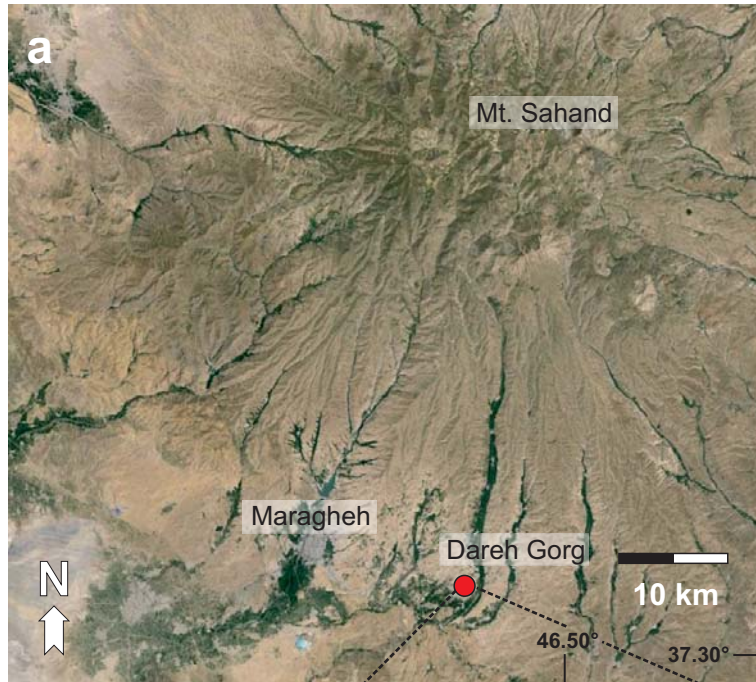
519

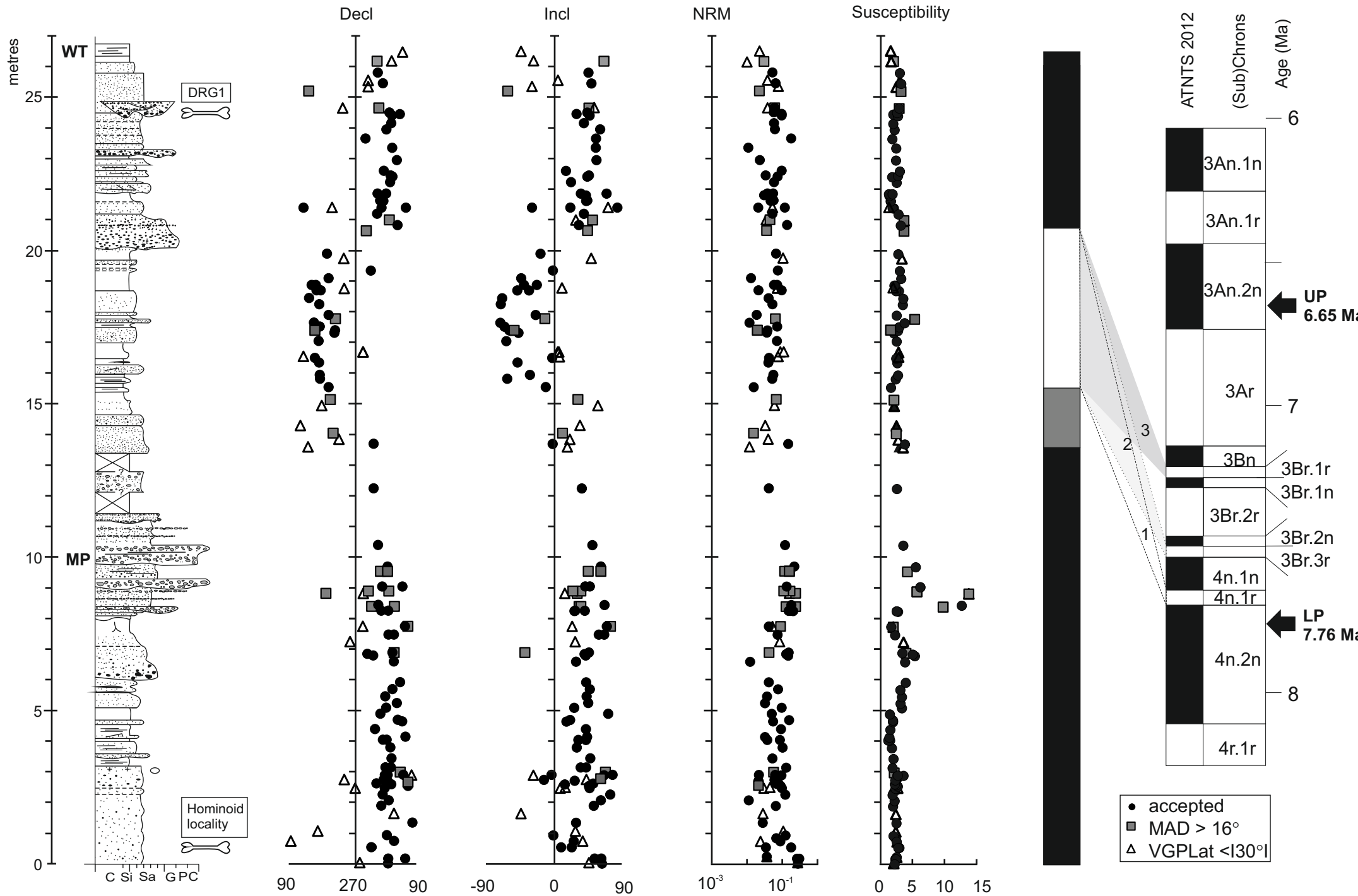
Table 1 Radiometric ages obtained for the Dareh Gorg section.

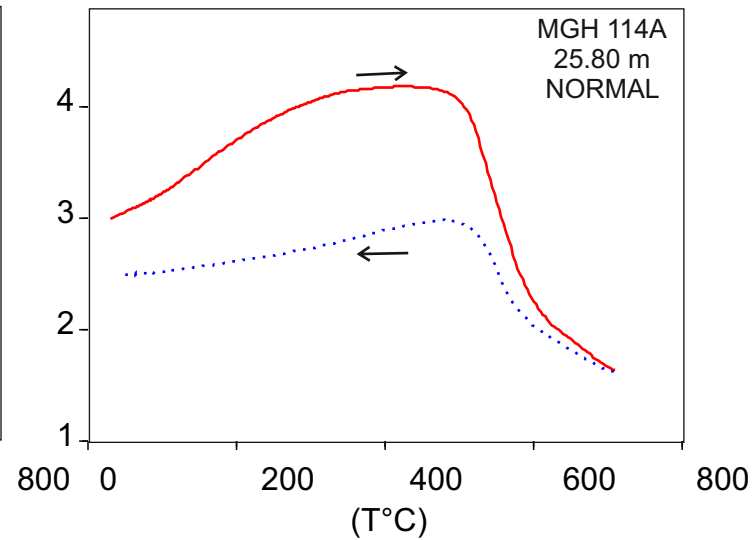
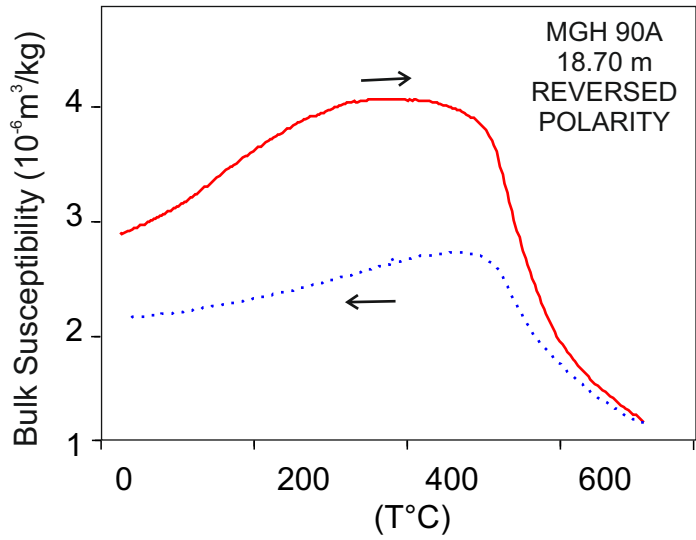
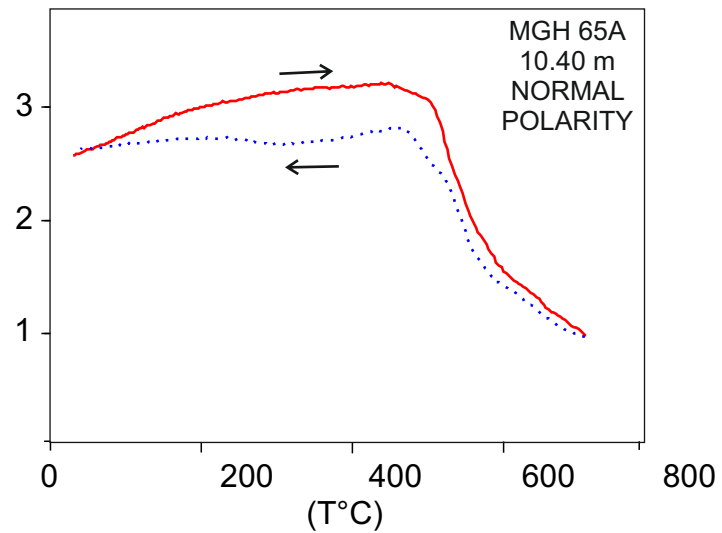
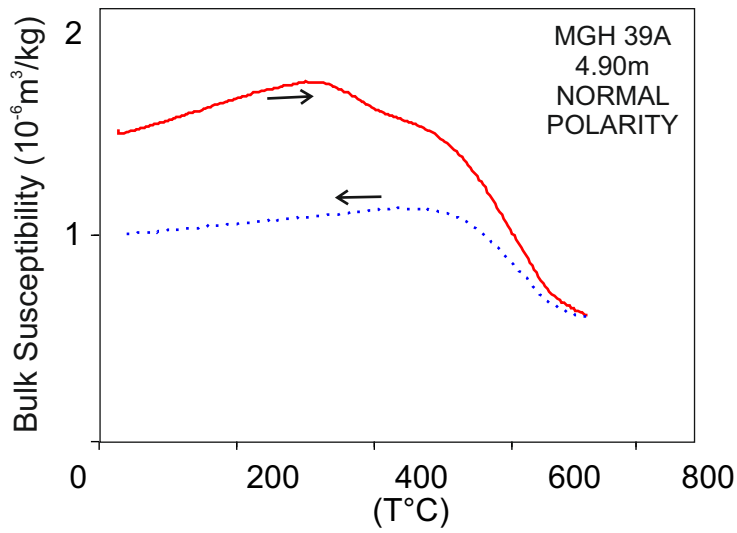
Method (mineral)	S	Ignimbritic tuff	Lower Pumice	Middle Pumice	Upper Pumice	Reference
		Age (Ma)	Age (Ma)	Age (Ma)	Age (Ma)	
Fission track (zircon)	△	7.0 ± 1.4		6.5 ± 1.3 ^a	6.6 ± 1.3	Kamei et al. 1977
K-Ar (pl)	□	8.9 ± 0.5				Bernor et al. 1980
		8.8 ± 0.5				
		6.4 ± 0.5				
Fission track	▲	10.6 ± 0.8				Bernor et al. 1980
Ar-Ar (pl)	●	8.645 ± 0.029				Swisher III et al. 1996
K-Ar mean (hbl, pl)	■	8.14 ± 0.27	7.54 ± 0.22 6.95 ± 0.28	7.87 ± 0.29	6.96 ± 0.31	Sawada et al. 2016 this volume (mean)

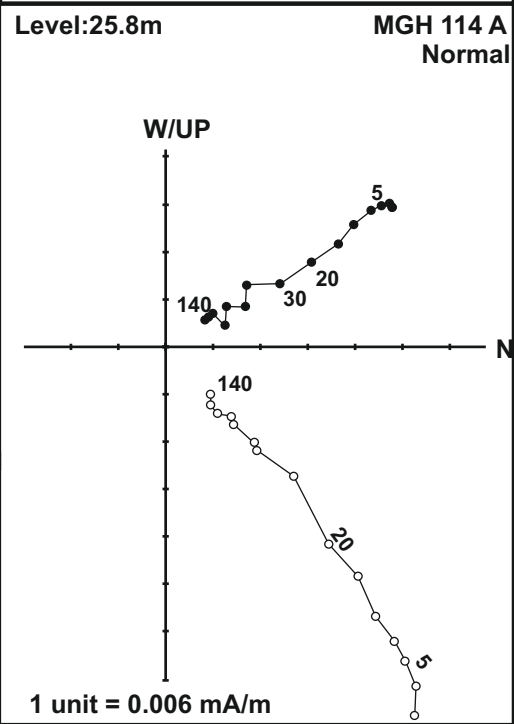
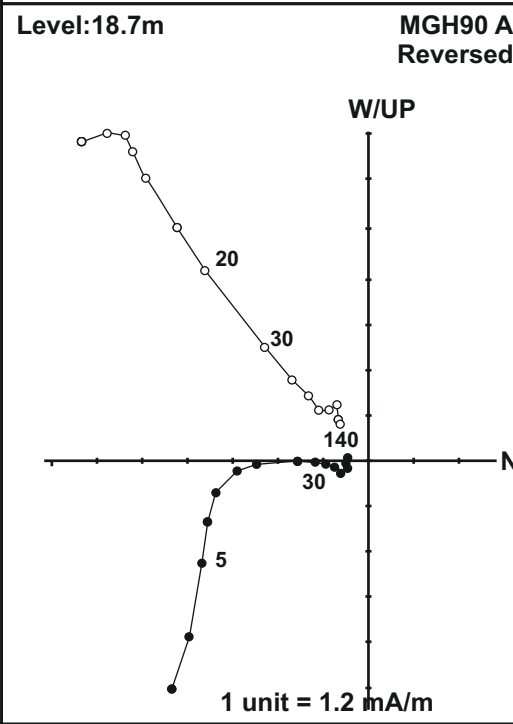
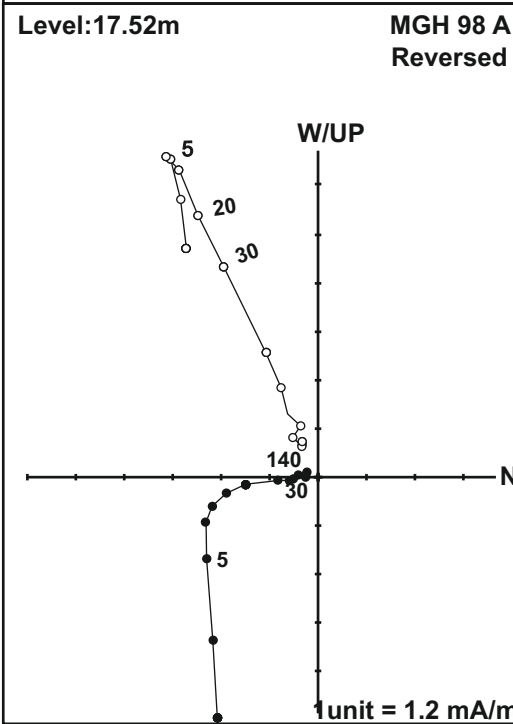
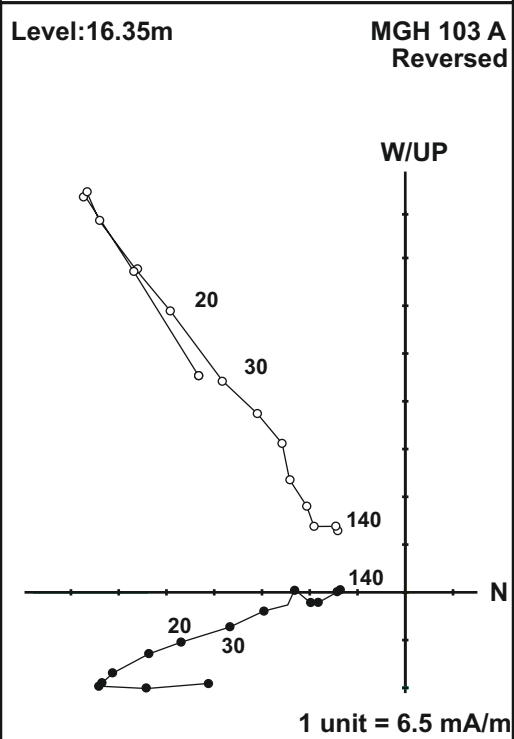
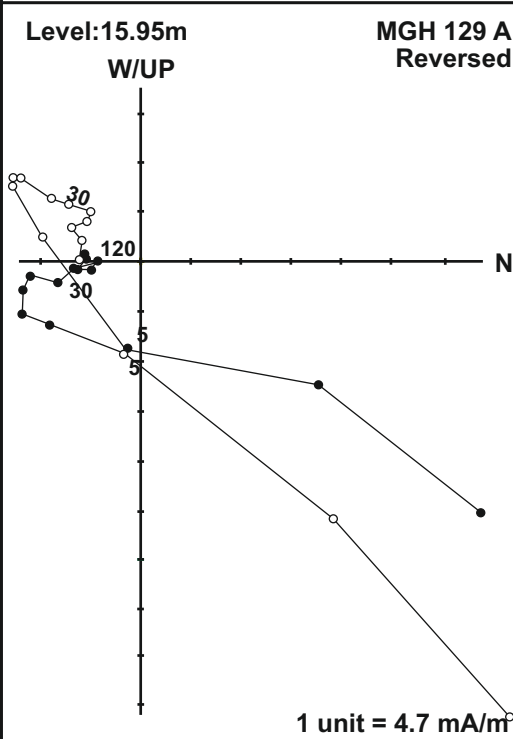
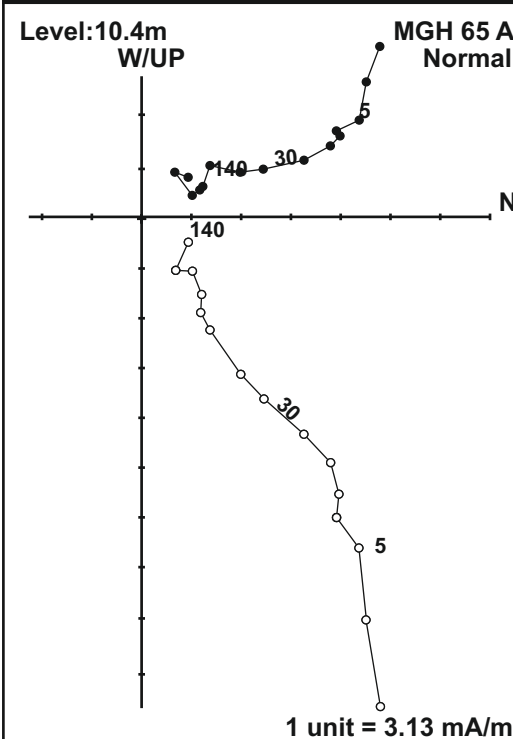
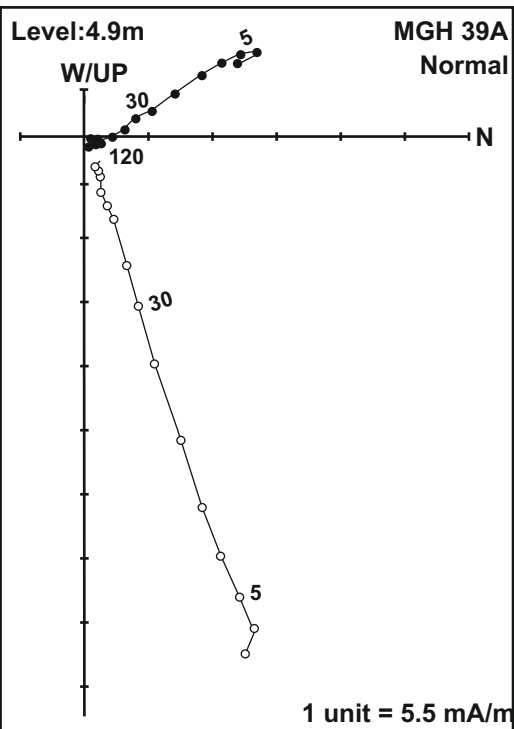
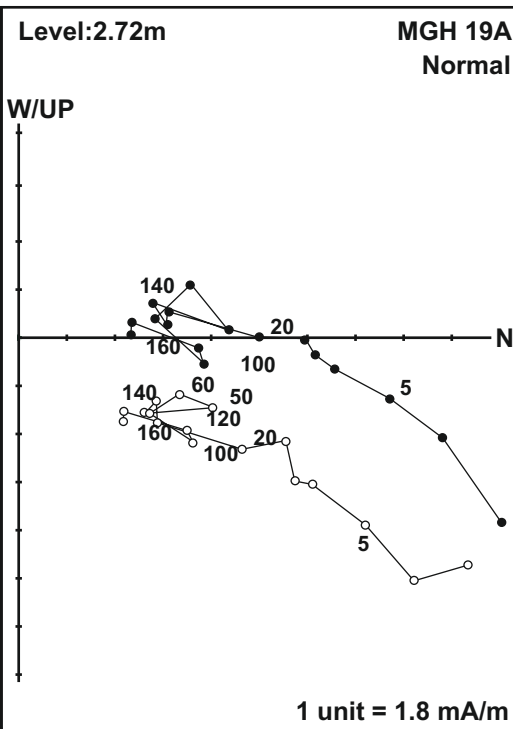
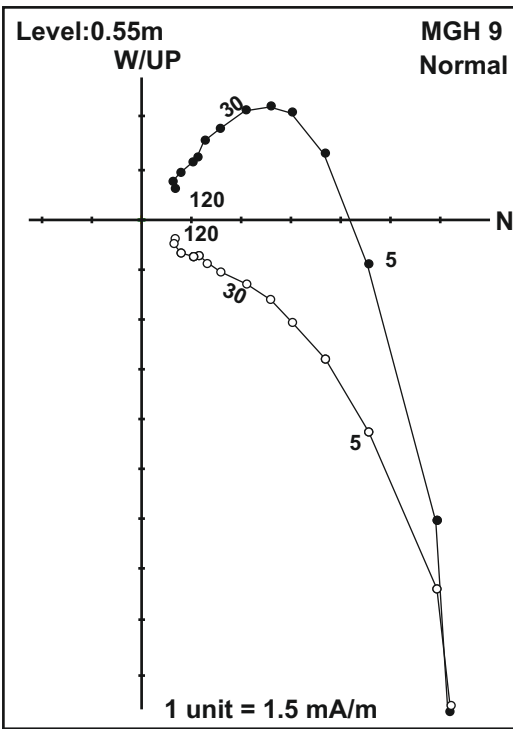
S symbol in Fig.7., *hbl* hornblende, *pl* plagioclase

^a Lower Pumice of Kamei et al. (1977)

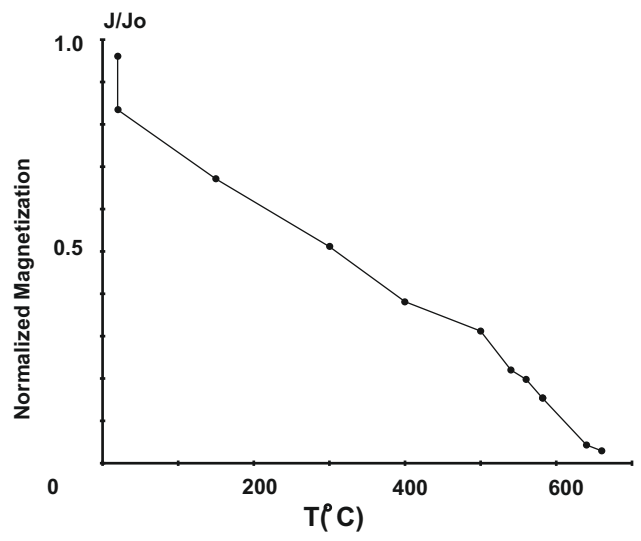
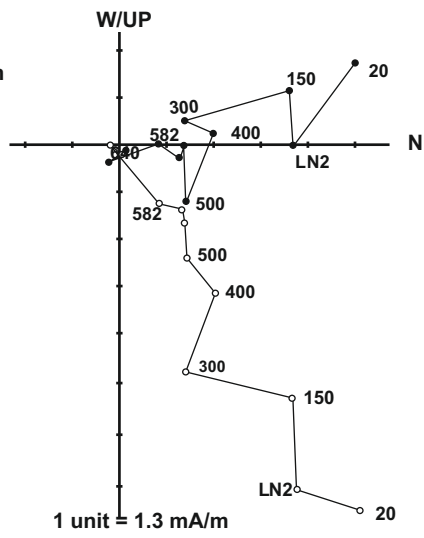








MGH 30B
Normal
Level:3.15m



MGH96 B
Reversed
Level:17.32m

